

also solidify the hypothesized compositional link between terrestrial komatiites and martian volcanism (20). The diversity of compositions recognized within the limited spatial coverage of the ISM data set and our demonstrated ability to “see through” the alteration and dust bodes well for expanding our knowledge and understanding of martian crustal compositions and processes from future Mars missions.

REFERENCES AND NOTES

1. B. C. Clark *et al.*, *J. Geophys. Res.* **87**, 10059 (1982).
2. P. J. Mouginiis-Mark, L. Wilson, M. T. Zuber, in *Mars*, H. H. Kieffer, B. M. Jakosky, C. W. Snyder, M. S. Matthews, Eds. (Univ. of Arizona Press, Tucson, 1992), chap. 13.
3. G. Schubert, S. C. Solomon, D. L. Turcotte, M. J. Drake, N. H. Sleep, *ibid.*, chap. 5; J. Longhi, E. Knittle, J. R. Holloway, H. Wänke, *ibid.*, chap. 6.
4. H. Y. McSweeney Jr., *Meteoritics* **29**, 757 (1994).
5. T. L. Roush, D. L. Blaney, R. B. Singer, in *Remote Geochemical Analysis: Elemental and Mineralogical Composition*, C. M. Pieters and P. A. J. Englert, Eds. (Cambridge Univ. Press, Cambridge, 1993), pp. 367–394; L. A. Soderblom, in *Mars*, H. H. Kieffer, B. M. Jakosky, C. W. Snyder, M. S. Matthews, Eds. (Univ. of Arizona Press, Tucson, 1992), chap. 17.
6. R. B. Singer and H. Y. McSweeney, in *Resources of Near-Earth Space*, J. Lewis, M. S. Matthews, M. L. Guerrieri, Eds. (Univ. of Arizona Press, Tucson, 1993), pp. 709–736; J. F. Mustard, S. L. Murchie, S. Erard, *Lunar Planet. Sci.* **XXIV**, 1039 (1993).
7. P. Pinet and S. Chevrel, *J. Geophys. Res.* **95**, 14435 (1990).
8. J.-P. Bibring *et al.*, *Nature* **341**, 591 (1989).
9. J. M. Sunshine, C. M. Pieters, S. F. Pratt, *J. Geophys. Res.* **95**, 6955 (1990).
10. S. Erard *et al.*, *Proc. Lunar Planet. Conf.* **21**, 461 (1991).
11. R. G. Burns, *Mineralogic Applications of Crystal Field Theory* (Cambridge Univ. Press, Cambridge, 1993).
12. J. F. Mustard *et al.*, *J. Geophys. Res.* **98**, 3387 (1993).
13. J. B. Adams, *ibid.* **79**, 4829 (1974); E. A. Cloutis and M. J. Gaffey *ibid.* **96**, 18819 (1991).
14. J. M. Sunshine and C. M. Pieters, *ibid.* **98**, 9075 (1993).
15. ———, *Lunar Planet. Sci.* **XXIV**, 1379 (1993); J. F. Mustard, *Am. Mineral.* **1992**, 345 (1992).
16. J. M. Sunshine, L. C. McFadden, C. M. Pieters, *Icarus* **105**, 79 (1993).
17. A. Tarantola and B. Valette, *Rev. Geophys. Space Phys.* **20**, 219 (1982).
18. H. Y. McSweeney and E. M. Stolper, *Geochim. Cosmochim. Acta.* **47**, 1501 (1983).
19. J. Longhi and V. Pan, *Proc. Lunar Planet. Sci. Conf.* **19**, 451 (1991).
20. This link has been proposed by many workers, including T. R. McGetchin and T. R. Smyth [*Icarus* **34**, 512 (1978)], Pinet and Chevrel (7), and D. P. Reyes and P. R. Christensen [*Geophys. Res. Lett.* **21**, 887 (1994)].
21. This manuscript is presented as a tribute to the late Roger G. Burns, whose fundamental research on mineral spectroscopy and martian geochemistry, as well as his encouragement and friendship, played an essential role in our research. We thank P. Hess and M. Rutherford for helpful discussions. This work was supported under National Aeronautics and Space Administration grant NAGW-3379 (J.F.M.).

25 October 1994; accepted 18 January 1995

Direct Observations of Excess Solar Absorption by Clouds

Peter Pilewskie* and Francisco P. J. Valero

Aircraft measurements of solar flux in the cloudy tropical atmosphere reveal that solar absorption by clouds is anomalously large when compared to theoretical estimates. The ratio of cloud forcing at an altitude of 20 kilometers to that at the surface is 1.58 rather than 1.0, as predicted by models. These results were derived from a cloud radiation experiment in which identical instrumentation was deployed on coordinated stacked aircraft. These findings indicate a significant difference between measurements and theory and imply that the interaction between clouds and solar radiation is poorly understood.

Evidence from several experimental and theoretical investigations over the past four decades has shown that the magnitude of shortwave (solar) absorption by clouds is uncertain. There has been some hint that solar absorption is in excess of that predicted by models (1). Cess *et al.* (2) and Ramanathan *et al.* (3) reported that the absorption by the entire atmospheric column in the presence of clouds exceeds model

predictions of absorption by perhaps 35 W m⁻² over the Pacific warm pool (3). The relative error this difference introduces into current theoretical estimates of solar absorption is large, considering that average clear-sky absorption in that region is about 100 W m⁻². The absolute error appears to be small when compared to other terms in the energy budget, but that is misleading. Most of the solar radiation absorbed in the tropics goes toward heating the surface; the remainder, about 20%, helps drive the atmospheric circulation. Thus, what appear to be small errors in absorption by the atmosphere might have huge consequences in tropical atmospheric dynamics. Another consequence of our inability to predict the

magnitude of solar absorption by clouds is the misinterpretation of remote sensing data used to infer cloud microphysical properties. In this report, we present measurements of cloud absorption from the Tropical Ocean Global Atmosphere–Coupled Ocean Atmosphere Response Experiment (TOGA-COARE) and the Central Equatorial Pacific Experiment (CEPEX), based on direct observations from aircraft. For consistency, we present our analysis in a manner similar to that used in (2, 3).

In TOGA-COARE and CEPEX, 20 coordinated flights were made with identical instrumentation above (at an altitude of ~20 km) and beneath (8 to 12 km) cloud layers to determine cloud energetics (that is, flux divergence, absorption, heating, and so on). From TOGA-COARE, 33 hours of useful solar radiation data were acquired during well-coordinated flight segments (aircraft within 0.5°). CEPEX provided an additional 18 hours of well-coordinated solar flux measurements. During both TOGA-COARE and CEPEX, the National Aeronautics and Space Administration (NASA) ER-2 aircraft flew at nearly constant altitude near the tropopause, approximately 20 km; in TOGA-COARE the NASA DC-8 flew at mid-troposphere altitude, between 8 and 12 km, and in CEPEX, the mid-troposphere aircraft was the Aeromet Learjet. Each aircraft was instrumented with two identical broadband (0.3 to 4.0 μm) solar hemispheric field-of-view radiometers (BBHFOV) for simultaneous measurement of upwelling and downwelling flux at both flight levels. Total direct-diffuse radiometers (TDDR) on each aircraft were used to measure spectral components of the solar flux (4, 5).

If one is to determine the absorption in a layer, net solar flux must be acquired simultaneously, or nearly so, at both flight altitudes (Fig. 1). Using the flight navigational data from the DC-8 (or Learjet, for CEPEX) and ER-2 aircraft, we shifted time series of flux data to best align the data sets. Typical time offsets between ER-2 and DC-8 (Learjet) data were less than 3 min, and in most cases the offset was negligible. Therein lies the advance in the TOGA-COARE and CEPEX data sets over the data obtained earlier. Most of the earlier experimental attempts at determining cloud absorption relied on a single aircraft making measurements at several flight altitudes. The reduction to cloud absorption then relied on knowledge of cloud advection, homogeneity, evolution, and so forth. Because flux divergence is obtained from the residual of two relatively large numbers, the net fluxes, coeval measurements are crucial to limiting errors. Some limited attempts have been made at flying stacked aircraft

P. Pilewskie, National Aeronautics and Space Administration Ames Research Center, Moffett Field, CA 94035, USA.

F. P. J. Valero, Atmospheric Research Laboratory, Scripps Institution of Oceanography, University of California at San Diego, La Jolla, CA 92093, USA.

*To whom correspondence should be addressed.

(6), but identical instruments with identical calibration were not used.

We reduced our data in a manner similar to that described in (2, 3) to examine column absorption in the presence of clouds. An important distinction between our measurements and those of (2) is that our net flux below cloud layers is between 8 to 12 km above the surface rather than at the surface. We adopted two methods for deducing the effect of absorption by clouds (2, 3): determination of (i) the ratio of cloud forcing above the cloud to cloud forcing beneath the cloud layer and (ii) the slope of cloud reflectance versus transmission.

Cloud forcing is defined as the difference between cloudy and clear-sky net flux. Cloud forcing beneath the cloud layer, C_S , is equivalent to the difference between absorption by the surface and the lower atmosphere under the clouds on the one hand and the absorption by the surface and the lower atmosphere under a clear column on the other. Cloud forcing above the cloud layer (in our case, at the tropical tropo-

pause), C_T , is the difference between absorption by the cloudy total-column atmosphere and surface versus that by the clear total-column atmosphere and surface. If the cloud forcing of the atmosphere column above the under-cloud level is denoted by C_A , then

$$C_T = C_A + C_S \quad (1)$$

and

$$C_S/C_T = C_S/(C_A + C_S) \quad (2)$$

The quantity C_A is given by

$$C_A = A(\text{cloud}) - A(\text{clear}) \quad (3)$$

where A is the absorption by the column. The ratio of C_S to C_T is unity when $A(\text{cloud})$ is equal to $A(\text{clear})$; model predictions place this ratio around unity, and rarely does it exceed 1.2 (3, 7), indicating a negligible difference in absorption between the clear and cloudy atmosphere. An important conclusion presented in (2, 3) is that the ratio might be substantially higher, implying that a significant discrepancy exists between model-predicted cloud (or more precisely, cloudy column) absorption and cloud absorption derived from measurements.

The most critical element needed to estimate cloud forcing is the clear-sky net flux because it cannot be determined concurrently with a cloudy-sky net flux measurement. Rather than use satellite-derived quantities, we determined clear-sky net flux from direct measurements [as in (2)]. We constructed a scatter diagram of all net flux (F_{net}) data versus the cosine of the solar zenith angle, ζ . By definition, the maximum values of F_{net} for a particular value of solar angle occur under clear conditions. However, under broken cloudy skies, downwelling solar flux can exceed the same flux under clear conditions if scattering from the sides of clouds becomes significant. With that in mind, we performed a linear regression analysis of the upper envelope of points to determine the relation between $F_{\text{net}}(\text{clear})$ and $\cos(\zeta)$. The geographical region covered during TOGA-COARE and CEPEX was extensive, between 140°E to 180°E and 15°S

to 0°S. However, the entire region is over the ocean surface and is part of the quasi-homogeneous warm-pool region, where sea-surface temperatures are between 300 and 303 K. The variability in humidity profiles above 10 km would not significantly affect clear-sky net flux over the region. We estimate the uncertainty of our clear-sky net flux to be $\pm 5 \text{ W m}^{-2}$.

Comparison of the clear-sky absorption between the two flight levels, approximately 10 to 20 km (solid line in Fig. 2), and 3-min averages of all column (cloudy and clear) absorption obtained from the difference of F_{net} measurements shows that, on average, cloud absorption far exceeds clear-sky absorption in the same layer. The average of the absorption was 165 W m^{-2} ; maximum absorption approaches 30% of the solar constant. A few of the cloud absorption points actually fall under the clear-sky absorption values, possibly the result of side-scattering from clouds producing an anomalously high value of DC-8 (Learjet) F_{net} .

The dependence of absorption on ζ is difficult to decipher from the 3-min averaged data (Fig. 2). To examine this dependence, we computed the average cloud absorption in 0.1-wide $\cos(\zeta)$ bins. Those values (Fig. 3) show a noticeable trend toward increasing absorption with increasing cosine, at a rate steeper than that for clear-sky absorption.

The predicted model estimate of C_S/C_T , unity, is not attained unless clear-sky and cloudy-sky absorption are identical. Our data (Figs. 2 and 3) show substantial differences between clear- and cloudy-sky absorption. However, the model estimates are based on surface cloud forcing, whereas we determined cloud forcing beneath clouds but at 10 km. Cosine-averaged values of $\langle C_S \rangle / \langle C_T \rangle$, shown in Fig. 4, were computed in a manner similar to the cosine-averaged absorption in Fig. 3. The average over all angles is 1.68. Using calculations of solar transmission in the lowest 10-km layer (8), we estimate that this is equivalent to a ratio $C_S(\text{surface})/C_T$ of 1.5. Our findings are thus consistent with those reported in (2, 3).

A more direct comparison with (2, 3) can

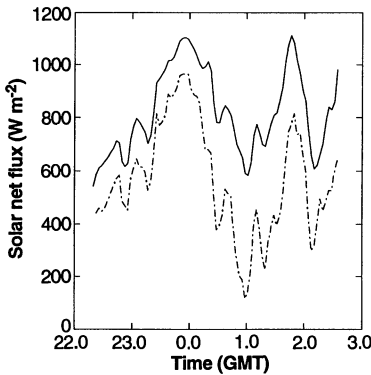


Fig. 1. Net solar flux measured at 20 km from the NASA ER-2 (solid curve) and at 10 km from the NASA DC-8 (dashed curve) over the tropical western Pacific during the TOGA-COARE flight on 31 January 1993.

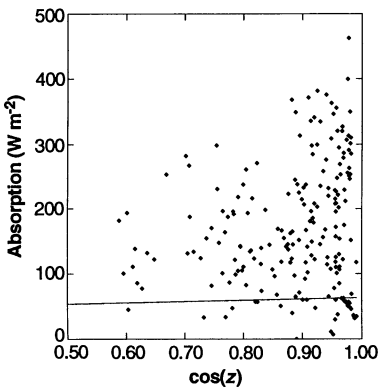
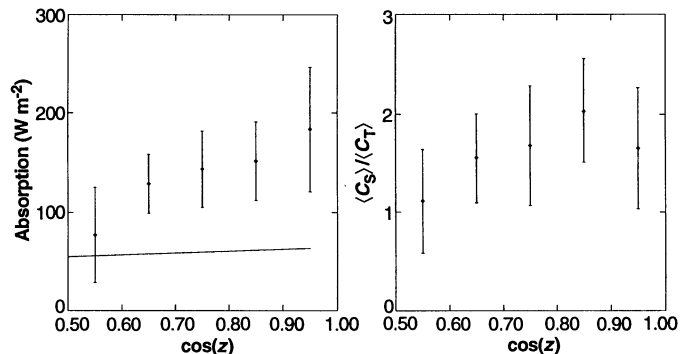


Fig. 2. Three-minute averages of cloud absorption determined by the difference between net flux at 20 km and at 10 km, from TOGA-COARE and CEPEX. The solid line indicates our estimate of clear-sky absorption.

Fig. 3 (left). Averages in 0.1-wide cosine bins of the absorption data shown in Fig. 2. The solid line indicates our estimate of clear-sky absorption. Error bars denote the standard deviation of the sample, a measure of the range of variability in observed cloud absorption.

Fig. 4 (right). Same as Fig. 3, except that the ordinate is the ratio $\langle C_S \rangle / \langle C_T \rangle$.



be made only by inferring the surface flux at the base of the column beneath the aircraft flight track. Using an estimate of the average clear-sky column absorption from (3) and making the plausible assumption that our estimate of average cloudy column absorption is somewhat independent of total column depth (9), we can make such an inference. Because of Eqs. 1 and 3,

$$C_S = C_T - A(\text{cloud}) + A(\text{clear}) \quad (4)$$

Our estimates of $A(\text{cloud})$ and C_T are 165 W m^{-2} and -113 W m^{-2} , respectively. Adopting the estimate of $A(\text{clear})$ over the tropical warm pool from (3), 100 W m^{-2} , we arrive at $(C_S)/(C_T) = 1.58$. We conclude that our estimates of cloud absorption are in considerable variance with model predictions (Fig. 5).

A further consequence of using flight data versus surface data is the variability in planetary albedo along a flight track. All of the TOGA-COARE flights were over the sea surface, and so variability in the reflectance at the altitude of the DC-8 was a direct measure of variability in cloud optical thickness and cloud cover beneath the aircraft. We therefore used our measurement of albedo from the DC-8 to dis-

criminate between clear and cloudy conditions beneath the cloud deck, adopting a threshold of 0.15. Although the albedo of the sea surface is considerably less, around 0.06 for overhead sun, completely clear conditions almost never occurred in that region of the tropics, particularly in the boundary layer, where scattered cumulus clouds were prevalent.

Several of the surface sites used by Cess *et al.* (2) had available only flux radiometers that viewed the zenith; thus, measurements of surface net flux were not possible. However, they were able to determine the relation between satellite-derived albedo at the top of the atmosphere (TOA) and the ratio of insolation at the surface to insolation at the TOA—that is, reflectance versus transmission. (In our case, below-cloud transmission was measured not at the surface but at a flight altitude of 10 km.) The slope of the fit of their data is ~ -0.6 , whereas model predictions are closer to -0.8 . The lower magnitude slope for the measured data indicates that solar absorption in the column was greater than typically derived in models.

For comparison, we examined the relation between cloud reflectance, measured at the tropopause from the ER-2, and cloud transmission, measured beneath cloud layers from the DC-8 (Learjet), flying between 8 and 12 km, using the 3-min averaged integrated solar flux data. Filtering of selected data (Fig. 6) was done on the basis of albedo measured from the DC-8 and a threshold of 0.15. For the 200 cases satisfying that condition, the resulting slope of the regression line (Fig. 6) is -0.48 . The variability of albedo measured from the DC-8 makes our analysis slightly different from that shown in (2), where stationary ground sites with fixed albedo were considered. The tendency toward higher surface albedo would increase the TOA albedo in the set of points arising from minimal cloudy conditions (to the right in Fig. 6). The consequence of measuring the transmission from the DC-8 (as opposed to measuring transmission at the surface) has a similar effect.

ceeds that measured at the surface, and this would also tend to decrease the slope.

Although the slope of our regression fit is less than that found by Cess *et al.* (2), it is consistent with their general results. Calculations of the atmospheric transmission between the surface and 10 km (8) show that the ground-based slope of -0.6 would fall to approximately -0.5 if surface transmission were replaced by transmission at 10 km. On the basis of these results as well as our estimate of the ratio of cloud forcing beneath clouds to that at the tropopause, it is evident that our findings are completely consistent with those of (2, 3) and that measured cloud absorption exceeds theoretical estimates.

Several factors that might contribute to the discrepancies between measured and calculated absorption by clouds have been postulated (1). One is cloud inhomogeneity (models are typically run for plane-parallel homogeneous cloud layers). Filtering of our data allowed us to examine cloud morphology and inhomogeneity. We averaged our flux measurements over 3-min periods to smooth higher frequency features that might otherwise lead to difficulties in interpreting data sets from the two aircraft platforms. The spatial resolution of the ER-2 and DC-8 data are not identical, owing to differences in the ranges of clouds from both aircraft, thus necessitating the use of time-averaged data. One measure of cloud homogeneity along the flight track is the standard deviation of the upwelling flux at ER-2 altitude (20 km) over the 3-min period. We segregated the data shown in Fig. 6 by filtering at 10 and 5% standard deviation in the upwelling flux at 20 km (Fig. 7). The slopes of the new regression lines are -0.54 and -0.61 for the 10 and 5% standard deviation thresholds, respectively. Undoubtedly, the effect of filtering is to reduce the cluster of lower albedo cases and to increase the slope of our fit. Whether this can be construed as indicating an increase in absorption with inhomogeneity remains uncertain. The statistical significance of the filtered data set is questionable because only 25% of all cases met the 5% standard deviation criterion.

If cloud morphology is the key to enhanced cloud absorption, do broken and variable clouds really increase column absorption (by changing photon path lengths) or is the effect only apparent and a measure of the inadequacy of current models to predict the scattering and absorption of real clouds? Other issues also remain unresolved. Do clouds absorb anomalously, or does there exist a different anomalous absorber, such as a carbon-based aerosol? Spectral data from the TOGA-COARE experiment suggest that this is not the case and that the significant absorption and scattering fea-

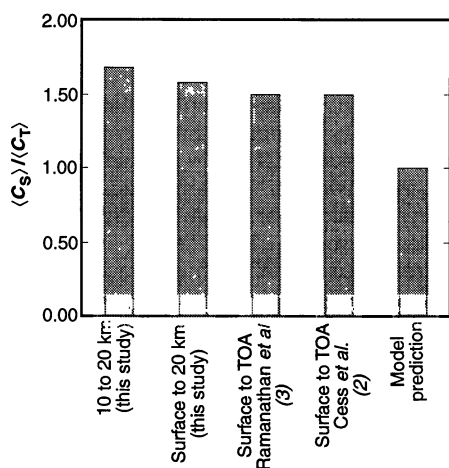
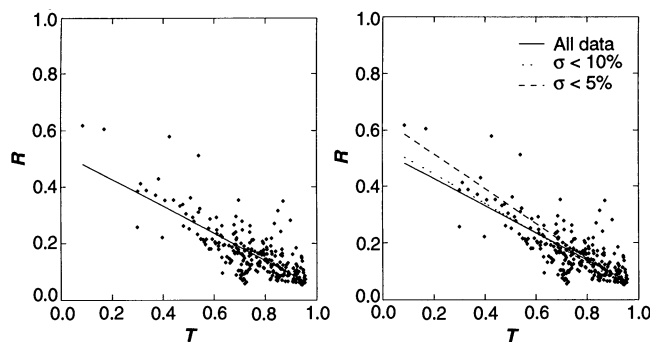


Fig. 5. Summary of estimates of $(C_S)/(C_T)$ determined by this study, (2, 3), and model calculations.

Fig. 6 (left). The ER-2 albedo or reflectance, R , as a function of DC-8 transmission, T . The solid line indicates the linear regression fit. The slope is -0.48 .

Fig. 7 (right). Same as Fig. 6, except that two more regression curves are plotted, derived from data that were filtered to remove values arising when the standard deviation of the ER-2 net flux exceeded 10 and 5%. The slopes of the new curves are -0.54 and -0.61 , respectively.



tures in the tropical atmosphere are water-like. Further examination of this point must rely on more spectral measurements, particularly in the near-infrared, where liquid water absorption and ice absorption become important.

REFERENCES AND NOTES

1. G. L. Stephens and S. Tsay, *Q. J. R. Meteorol. Soc.* **116**, 671 (1990).
2. R. D. Cess *et al.*, *Science* **267**, 496 (1995).
3. V. Ramanathan *et al.*, *ibid.*, p. 499.
4. F. P. J. Valero *et al.*, *Geophys. Res. Lett.* **10**, 1184 (1983); F. P. J. Valero *et al.*, *ibid.* **11**, 465 (1984).
5. The BBHFOV covered the entire hemisphere. Response time was 1 ms. The BBHFOV was calibrated versus a cavity radiometer, resulting in an absolute accuracy of 1%. The TDDR also had a hemispheric field of view but had seven discrete, narrow bandwidth (10-nm) channels throughout the visible and near-infrared. When the TDDR "looked" in the zenith direction, an oscillating shadow arm blocked the direct downwelling solar flux once per cycle (30 s); this variation allowed measurement of both the diffuse and the direct components of solar flux. Our study focuses on the spectral flux capabilities of the TDDR and, in particular, spectral hemispherical reflectance obtained from a nadir-viewing TDDR.
6. J. S. Foote and F. Rawlins, *IAMAP 89, Fifth Scientific Assembly of the International Association of Meteorology and Atmospheric Physics, Brief Review Papers and Abstracts*, B. W. Riddaway, Ed. (31 July to 12 August 1989, University of Reading, Reading, United Kingdom).
7. Z. Q. Li *et al.*, *J. Climate* **6**, 317 (1993).
8. We used the LOWTRAN7 atmospheric transmission model to calculate solar transmission between the surface and 10 km.
9. This is directly related to the issue of cloud absorption versus cloudy-column absorption. We are assuming that, as a result of the diffuse scattering by clouds, the strong water vapor bands are already saturated in the 10- to 20-km column such that the lower 10 km will not add appreciably to the total column absorption. Of course, this effect will depend on cloud thickness and geometry and potential absorbing aerosols in the lower troposphere.
10. This research was supported under NASA program code 460-42 and NSF grant 9223467.

31 October 1994; accepted 17 January 1995

Self-Assembled Metal Colloid Monolayers: An Approach to SERS Substrates

R. Griffith Freeman, Katherine C. Grabar, Keith J. Allison, Robin M. Bright, Jennifer A. Davis, Andrea P. Guthrie, Michael B. Hommer, Michael A. Jackson, Patrick C. Smith, Daniel G. Walter, Michael J. Natan*

The self-assembly of monodisperse gold and silver colloid particles into monolayers on polymer-coated substrates yields macroscopic surfaces that are highly active for surface-enhanced Raman scattering (SERS). Particles are bound to the substrate through multiple bonds between the colloidal metal and functional groups on the polymer such as cyanide (CN), amine (NH₂), and thiol (SH). Surface evolution, which can be followed in real time by ultraviolet-visible spectroscopy and SERS, can be controlled to yield high reproducibility on both the nanometer and the centimeter scales. On conducting substrates, colloid monolayers are electrochemically addressable and behave like a collection of closely spaced microelectrodes. These favorable properties and the ease of monolayer construction suggest a widespread use for metal colloid-based substrates.

In SERS, millionfold enhancements in Raman scattering can be obtained for molecules that are adsorbed at suitably rough surfaces of Au, Ag, and Cu (1). Although many approaches have been reported (2), preparation of well-defined, stable SERS substrates having uniform roughness on the critical scale of 3 to 100 nm has proven difficult. Because colloidal Au can be synthesized as monodisperse solutions throughout most of this size regime (3) and because molecules adsorbed to closely

spaced, colloidal Au and Ag exhibit enhanced Raman scattering (4), these particles are excellent building blocks for SERS-active substrates.

The key issue is whether colloidal Au and Ag particles can be organized into macroscopic surfaces that have a well-defined and uniform nanometer-scale architecture. Indeed, controlling nanostructure is currently a central focus throughout materials research (5). Progress in the self-assembly of organic thin films on metal surfaces (6) led us to explore the reverse process: the self-assembly of colloidal Au and Ag particles onto supported organic films. As detailed below, this approach has yielded surfaces that are SERS-active, characterizable at both the macroscopic and the microscopic levels, highly reproducible, electrochemically addressable,

and simple to prepare in large numbers. Moreover, these substrates have a surface roughness that is defined by the colloid diameter (which is tunable) and an average interparticle spacing that is continuously variable. As such, self-assembled Au and Ag colloid monolayers are likely to have extraordinary utility for SERS.

Our construction protocol for SERS-active Au and Ag colloid monolayers exploits the simplicity of self-assembly from solution and the affinity of noble metal surfaces for certain organic functional groups (Fig. 1). In our case, these moieties are present by virtue of organic films either polymerized or deposited on the surface of macroscopic (≈ 0.8 cm by 2 cm) substrates. Immersion of the functionalized substrate into a dilute solution of monodisperse colloidal Au or Ag particles leads to colloid immobilization. This solution-based process is extremely general, encompassing numerous permutations of insulating and conducting substrates (glass, quartz, plasma-treated Teflon, Formvar, indium-doped SnO₂, and Pt), organic films [hydrolyzed mono-, di-, and trialkoxysilanes containing the functional groups CN, NH₂, 2-pyridyl, P(C₆H₅)₂, and SH, as well as carboxyl-terminated C₁₈ organothiol self-assembled monolayers], and colloids (5 to 70 nm in diameter for Au and 5 to 20 nm in diameter for Ag and Au-Ag composites) (7, 8).

Solution-based surface assembly also eliminates preparative, geometric, and operational constraints associated with most previously described SERS substrates (1, 2). Thus, 1 liter of 17 nM, 12-nm-diameter colloidal Au, which can be stored indefinitely at room temperature, can be used to prepare 2000 0.5-cm² surfaces with only a 1% decrease in colloid concentration. Importantly, these substrates can be assembled sequentially or simultaneously. Surfaces in novel geometries that extend the utility of SERS can now be derivatized, including one face of a 5- μ m spectroelectrochemical cell, large glass sheets several centimeters on a side, and the inside of a glass capillary with an inner diameter of 20 μ m (8). Moreover, once constructed, no further activation steps (such as electrochemical oxidation-reduction cy-

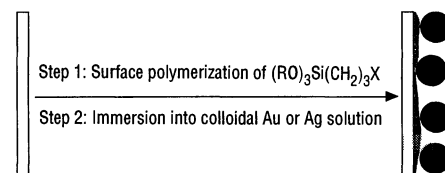


Fig. 1. Assembly strategy for Au and Ag colloid monolayers; X = CN, NH₂, 2-pyridyl, P(C₆H₅)₂, or SH; R = CH₃ or CH₂CH₃.

R. G. Freeman, Division of Science, Northeast Missouri State University, Kirksville, MO 63501, USA. K. C. Grabar, K. J. Allison, R. M. Bright, J. A. Davis, A. P. Guthrie, M. B. Hommer, M. A. Jackson, P. C. Smith, D. G. Walter, M. J. Natan, Department of Chemistry, The Pennsylvania State University, 152 Davey Laboratory, University Park, PA 16802, USA.

*To whom correspondence should be addressed.